Stokes geometry for the quantized Henon map (Recent Trends in Exponential Asymptotics)

AUTHOR(S):

Shudo, Akira

CITATION:

Shudo, Akira. Stokes geometry for the quantized Henon map (Recent Trends in Exponential Asymptotics). 数理解析研究所講究録 2005, 1424: 184-199

ISSUE DATE:

2005-04

URL:

http://hdl.handle.net/2433/47228

数理解析研究所講究録 1424 巻 2005 年 184-199

Stokes geometry for the quantized Hénon map

Akira Shudo

Department of Physics, Tokyo Metropolitan University,
1-1 Minami-Ohsawa, Hachioji, Tokyo 192-0397, Japan
shudo@phys.metro-u.ac.jp

1, The Hénon map and its quantum propagator

The Hénon map is a polynomial diffeomorphism given by:

$$f_a : \begin{pmatrix} x \\ y \end{pmatrix} \mapsto \begin{pmatrix} y \\ y^2 - x + a \end{pmatrix}. \tag{1}$$

We have a classification theorm claiming that non-trivial polynomial diffeomorphisms from $\mathbb{C}^2$ to $\mathbb{C}^2$ is written as a composition of the Hénon map, and the others, which are either elementary or affine map, are the mappings easily analyzed [1]. For this reason, the Hénon map can be regarded as a simplest possible polynomial diffeomorphism creating non-trivial dynamics.

An alternative familiar form is obtained by making an affine change of variables as $(p, q) = (y - x, x - 1)$ together with a parameter $c = 1 - a$,

$$F_c : \begin{pmatrix} q \\ p \end{pmatrix} \mapsto \begin{pmatrix} q + p \\ p - V'(q + p) \end{pmatrix}. \tag{2}$$

Here the potential function $V(q)$ is given as

$$V(q) = -\frac{q^3}{3} - cq. \tag{3}$$

The Hénon map (1) has a nonlinear paremeter a (or c) controling the dynamics qualitatively. When $a \gg 1$, the so-called horseshoe condition is satisfied and the mapping is conjugate to the symbolic dynamics with the binary full shift. All the stable and unstable manifolds for periodic orbits intersect transversally when the horsehoe is realized, and the system keeps hyperbolicity. Non-wondering set forms fractal repeller on the real plane.

A standard recipe to formulate quantum mechanics of the symplectic mapping is first to construct the unitary operator generating the time evolution of quantum states [2]. This is achieved by introducing discrete analog of the Feynman-type path integral:

$$< q_n|U^n|q_0 >= \int_{-\infty}^{\infty} \cdots \int_{-\infty}^{\infty} dq_1 dq_2 \cdots dq_{n-1} \exp\Big[\frac{i}{\hbar} S(q_0, q_1, \cdots, q_n)\Big]. \tag{4}$$

Here we take the coordinate representation. The function $S(q_0, q_1, \cdots, q_n)$ represents the discretized Lagrangian or the action functional given by

$$S(q_0, q_1, \cdots, q_n) = \sum_{j=0}^{n-1} \frac{1}{2}(q_{j+1} - q_j) - \sum_{j=1}^{n-1} V(q_j). \tag{5}$$

The action functional is derived so that applying the variational principle to $S(q_0, q_1, \cdots, q_n)$ generates the symplectic map (2). In fact, we can easily see that the condition

$$\frac{\partial S(q_0, q_1, \cdots, q_n)}{\partial q_j} = 0, \quad (1 \leq j \leq n-1), \tag{6}$$

yields the classical map in the Lagrangian form,

$$(q_{i+1} - q_i) - (q_i - q_{i-1}) = q_i^2 + c. \tag{7}$$

A usual (complex) semicalssical scheme is just to take the leading order contribution in evaluating the multiple integral $< q_n|U^n|q_0 >$ by stationary phase(or saddle point) method. The resulting semiclassical formula is expressed as a sum over contributions of classical trajectories connecting the initial and final states:

$$< q_n|U^n|q_0 > \approx \sum_{\gamma} A_\gamma(q_n, q_0) \exp\{\frac{i}{\hbar} S_\gamma(q_n, q_0) - i\mu_\gamma \frac{\pi}{2}\}, \tag{8}$$

where $A_\gamma(q_n, q_0)$ stands for the amplitude factor associated with quantum fluctuation around each classical path γ. $S_\gamma(q_n, q_0)$ is given by putting the data of the corresponding classical path γ into the action functional $S(q_0, q_1, \cdots, q_n)$, and μ_γ represents the Maslov index. The summation is taken over such classical orbits that are located initially on the manifold $q_0 = \alpha$, and finally on $q_n = \beta$, where both α and β should take real values since they are observables in the representation under consideration.

We remark that even if there exist no *real orbits* connecting the initial and final manifolds $q_0 = \alpha$ and $q_n = \beta$, we always have *complex orbits*, which appear as saddle point solutions of (6) with the conditions $\alpha, \beta \in \mathbb{R}$. Physically, such complex orbits can be and should be regarded as *tunneling orbits* since the transition between initial and final manifolds is forbidden within *real* classical orbits. This type of tunneling transition is often called *dynamical tunneling* in the literature [3, 4, 5].

2. Stokes geometry

Our motivation to investigate the quantized Hénon map is to clarify how chaos in the complex space controls quantum tunneling, and to establish the theory of *chaotic tunneling* [6, 7]. A special advantage to employ the Hénon map is that the theory of complex dynamical systems has well been developed for polynomial diffeomorphisms [8, 9]. This is important because the saddle point solutions of the quantum propagator are just the classical trajectories in the complex plane, especially tunneling transitions are in question. It is thus crucial to know the nature of complex classical dynamics, and also in this respect, the Hénon map is most suitable. In particular, recent series of works by Bedford and Smillie, based on the pluriharmonic theory in several complex variables, established various fundamental frameworks for higher dimensional diffeomorphism complex Hénon map [8]. In fact, as a direct outcome of their works, it has rigrously been proved that the most relevant family of complex orbits to describe dynamical tunneling is closely related with the *Julia set* [10]. Moreover, in the present

context, we should say more about the results by Bedford and Smillie since their fundametal statement on the convergency of invariant sets is applicable to the system with mixed phase space [8], in which dynamical tunneling most naturally appears.

On the other hand, as is well known, in applying the saddle point method, one must take into account *Stokes phenomena*, that is, not all the saddle point solutions(=complex classical orbits) do not contribute to the final semiclassical superposition (8), but only the solutions controlled by the connection through Stokes phenomena do so. The aim of this report is to present a recipe to introduce proper Stokes geometry to the quantum propagator (4) of the Hénon map and how it should be treated.

In what follows, we shall fix the initial coordinate $q_0 = \alpha$ and regard the quantum propagator (4) as a function of the final coordinate q_n. We therefore use the notation $I(q_n) \equiv < q_n|U^n|q_0 >$ to represent the multiple integral defined in eq. (4). As will be seen below, except for the argument on the Stokes geometry depending on several parameters in the Hénon map, we put aside q_0 dependence for the moment.

The Stokes phenomenon for the 1-step quantum propagator is almost trivial, since the single integral $I(q_2)$ can be transformed into a canonical form of the Airy integral by an appropriate change of variables. For $n \geq 3$, the object we have to analyze is multiple integrals. As easily anticipated, difficulties to understand Stokes phenomena in multiple integrals much escalate. Recent progresses in exact WKB analysis, however, provide us promising approach to such issues [11]. In particular, the work by Howls on the development of hyperasymptotic expansions in multiple integrals is directly connected with the present problem [12].

We shall actually study Stokes phenomena in our integrals using hyperasymptotic expansion in the following section. Before doing this, we here connect our problem to the treatment of Stokes phenomena in higher-order differential equations. This looks somewhat a redundant way, since in usual cases integral representations carry much more information than differential equations. However, in multiple integrals, even if they certainly take integral forms it is not trivial at all to see how the saddle point method should be applied or in which co-dimensional space Stokes phenomena occurs. In particular, although what we need is to know how the connection occurs in $I(q_n)$ as a function of q_n, little is known about how the Stokes geometry should be constructed in such a situation.

To this end, we here follow the work by Aoki, Kawai and Takei [13], in which they have provided a prescription to analyze Stokes phenomena in higher-order differential equations, say $P(x, \eta^{-1}d/dx)\psi(x) = 0$, within the exact WKB framework [13]. Their work contains not only a mathematical justification of the preceding work [14] in which *new Stokes curves* should be introduced in order to recover the univaluedness around crossing points of ordinary Stokes curves in an ad-hoc way, but also claims that *virtial turning points* (they are originally called new turning points in [13]) should first be taken into account to construct complete Stokes geometry. They also clarified that new Stokes curves play essentially the same part in the Stokes geometry.

The argument of [13] starts with defining virtual turning points as self-intersection points of bicharacteristic curves for the Borel transformed differential equation. Here self-intersection points are obtained by projecting full bicharacteristic strip onto (x, y)

plane, where the variables y denotes the variable dual to a large parameter η. Then new Stokes curves are defined as the ones emanating from virtual turning points.

In order to apply the same recipe to our integral $I(q_n)$, we here show; (i) the principal symbol, which gives the bicharacteristic equation of the Borel transform of differential operator, and (ii) a set of differential operator acting on our integral $I(q_n)$. Detailed derivations are given elsewhere [15]. We just present the final expression. For the principal symbol we have,

$$\sigma(\hat{\mathcal{H}})(q_n, S, \xi, \eta) \equiv -\eta \hat{H}(q_1, q_2) \left| \begin{array}{l} \\ q_1 = q_1(q_{n-1}, q_n) \\ q_2 = q_2(q_{n-1}, q_n) \end{array} \right|_{q_{n-1}=q_n-\xi\eta^{-1}} \tag{9}$$

where

$$\hat{H}(q_1, q_2) \equiv \frac{\partial}{\partial q_1} S(q_0, q_1, \cdots, q_n)\big|_{q_0=0} = 2q_1 + q_1^2 - q_2 + c, \tag{10}$$

and $\xi \equiv \eta p_n = \eta(q_n - q_{n-1})$. We note that q_1, which is a canonical conjugate variable to q_0, plays the role of time in the bicharacteristic curve.

Explicit forms of principal symbols $\sigma(\hat{H})(q_n, S, \xi, \eta)$ are given respectively as

$$\sigma(\hat{H}) = \eta^{-1}\xi^2 - 2(q_2 + 1)\xi + (q_2^2 + q_2 - q_0 + c)\eta \tag{11}$$

for $n = 2$, and

$$\begin{aligned} \sigma(\hat{H}) &= \eta^{-3}\xi^4 - 4(q_3 + 1)\eta^{-2}\xi^3 + (6q_3^2 + 10q_3 + 2c + 6)\eta^{-1}\xi^2 \\ &- (4q_3^3 + 8q_3^2 + 4cq_3 + 8q_3 + 4c + 3)\xi \\ &+ (q_3^4 + 2q_3^3 + 2cq_3^2 + 3q_3^2 + 3cq_3 + q_3 + c^2 + 3c - q_0)\eta \end{aligned} \tag{12}$$

for $n = 3$.

We also have explicit forms of differential equations for $n = 2$,

$$\left[\frac{d^2}{dq_2^2} - 2\eta(q_2 + 1)\frac{d}{dq_2} + \eta^2(q_2^2 + q_2 - q_0 + c) + \eta)\right] I(q_2) = 0. \tag{13}$$

Similarly, we obtain for $n = 3$ [16],

$$\begin{aligned} &\left[\frac{d^4}{dq_3^4} - 4\eta(q_3 + 1)\frac{d^3}{dq_3^3} + \left\{(6q_3^2 + 10q_3 + 2c + 6)\eta^2 - 6\eta\right\}\frac{d^2}{dq_3^2}\right. \\ &+\left\{(-4q_3^3 - 8q_3^2 - 4cq_3 - 8q_3 - 4c - 3)\eta^3 + (12q_3 + 10)\eta^2\right\}\frac{d}{dq_3} \\ &+\left\{(q_3^4 + 2q_3^3 + 2cq_3^2 + 3q_3^2 + 2cq_3 + q_3 + c^2 + 3c - q_0)\eta^4\right. \\ &\left.\left.+(-6q_3^2 - 8q_3 - 2c - 4)\eta^3 + 3\eta^2\right\}\right] I(q_3) = 0. \end{aligned} \tag{14}$$

Since we now have differential equations for our multiple integral (4), we apply a prescription for higher-order differential equations. Concerning turning points, we say

the point q_n^T is a turning point in the ordinary sense if the equation $\sigma(\tilde{\mathcal{H}}) = 0$ for ξ has a double root. In this case, we have,

$$\frac{dq_n^T(q_0, q_1)}{dq_1} = 0,$$
$$\frac{dS(q_0, q_1, \cdots, q_n^T(q_0, q_1))}{dq_1} = 0.$$

Also we follow the definition of virtual turning points, that is, for $q_1^{(i)} \neq q_1^{(j)}$, q_n^T is a virutal turning point if

$$q_n^T(q_0, q_1^{(i)}) = q_n^T(q_0, q_1^{(j)})$$
$$S(q_0, q_1^{(i)}, \cdots, q_n^T(q_0, q_1^{(i)})), = S(q_0, q_1^{(j)}, \cdots, q_n^T(q_0, q_1^{(j)})).$$

In the same way, we can apply the definition of Stokes curves. Recalling the generating relation, $\partial S(q_1, \cdots, q_n)/\partial q_n = p_n$, we say the curves emanating from the turning points q_n^T and satisfying the following relation;

$$\mathrm{Im}\, S(q_0, q_1^{(i)}, \cdots, q_{n-1}^{(i)}, q_n^T) = \mathrm{Im}\, S(q_0, q_1^{(j)}, \cdots, q_{n-1}^{(j)}, q_n^T). \tag{15}$$

Stokes curves emanating from ordinary turning points give the ordinary Stokes curves, and those from virtual turning points give new Stokes curves.

3. Stokes graphs and Stokes geometry for 2- and 3-step propagators

In this section, we shall present several concrete examples of Stokes graphs for the quantum propagator (4) and how one can complete the Stokes geometry. The first non-trivial Stokes graphs appear when we consider the quantum propagator for $n = 3$, in which four saddles appear as a solution of the saddle point condition, each of which is denoted by u_1, u_2, u_3, u_4 hereafter.

An example shown in Fig. 1 is the case with a certain generic a, meaning that ideal situations such as the horseshoe condition or hyperbolicity are not realized in the corresponding classical dynamics. The Lagrangian manifold on the real plane is depicted in Fig. 2. We can see that there exists one folding point, although stretching and folding processs is repreated twice. This is because another two folding points fall into the complex domain, and cannot appear in the real plane. In Fig. 1, we have drawn ordinary Stokes curves together with new Stokes curves. There are three ordinary turning points, two of which are situated on the complex domain, reflecting the aspect just mentioned. From each ordinary turning point, three ordinary Stokes curves emanate. We notice that not only simple crossing points denoted as a, a', b, b' in Fig. 1, but also a degenerated crossing point, on which three ordinary Stokes curves cross each other at a single point. This is not generic event since only two Stokes curves are naturally expected to intersect. Obviously, this is due to the symmetry with respect to the real axis.

We note that the situation is slightly complicated as compared with the case studied by Berks *et al.* Around simple crossing points in our Stokes graphs, for example the

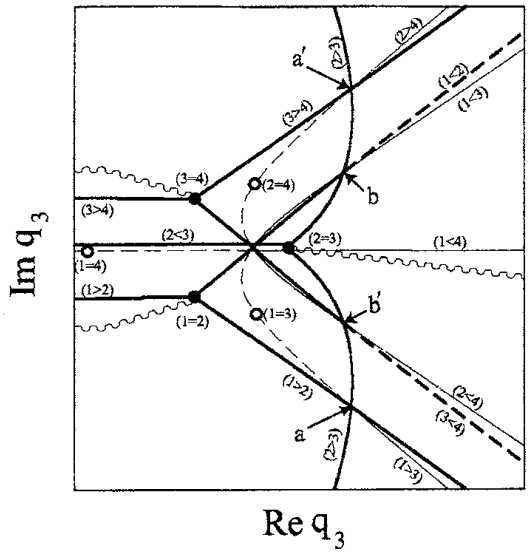

Figure 1: Complete Stokes geometry for the Hénon map propagator with $n = 3, c = 1, and q_0 = 0$. The solid and open circles denote the ordinary and virtual turning points respectively. Ordinary Stokes curves are drawn as thick lines and new ones as thin lines. The broken segments represent the parts of Stokes curves on which where no connections occur. The dominance relation on Stokes curves are indicated as $(i > j)$ meaning that the saddle i is dominant to that of j. One of ordinary Stokes lines emanating from the turning point $(2 = 3)$ and the new Stokes curve for the saddles 1 and 4 degenerate on the $\mathrm{Re}\, q_3$ axis. They are slightly shifted for clarity.

points denoted by a and a', which appear as a symmetric pair with respect to $\mathrm{Re}\, q_3$ axis, we know that the connection should occur on the segments on which ordinary and virtual turning points are located, but the rest of segements cannot be determined only after determining the connections around these crossing points. In order to know the characters of the remaining parts, we need to solve the connection problem around the degenerated crossing point. Similarly, the connection problem around simple crossing points b and b' remains unknown until the connetion around the degenereted crossing point will be decided.

Accordingly, we have first to solve the connection problem around the degenerated crossing point on the $\mathrm{Re}\, q_3$ axis. As expected, in addition to three ordinary Stokes curves, three new Stokes curves pass through the degenerated crossing point. The principle we have to impose is the same as employed in the case of simple crossing points, namely univaluedness condition around a given crossing point. As shown in Fig. 3, the characters on the segments that are directly connected to ordinary or virtual turning points are known in advance.

Once the connection around the double crossing point is fixed, the connection problems around the rest of single crossing points are automatically solved. In fact, as for

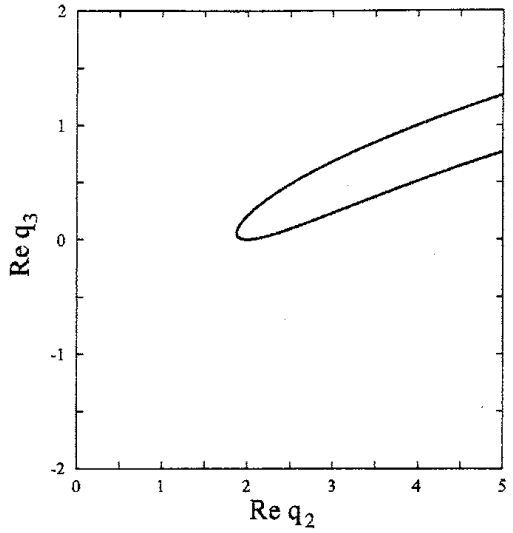

Figure 2: Lagrangian manifold for $n = 3$, The nonlinear parameter for the Hénon map is taken as $c = 0$. The initial manifold is given as $q_0 = 0, -\infty < q_1 < \infty$. There appears one caustic on the real plane but the others fall into the imaginary plane.

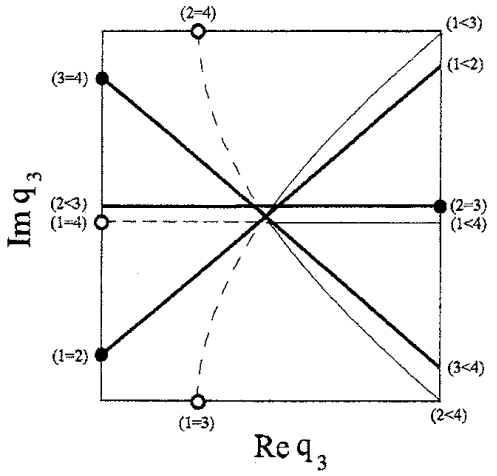

Figure 3: Magnification of complete Stokes geometry around the degenerated crossing point located on the Re q_3 axis. The degenerated Stokes curves on the Re q_3 axis are slightly shifted each other.

the crossing points a and a', characters of Stokes curves on one side is known, which allows one to determine characters beyond crossing points. The same is true for the crossing points b and b'. As a result, as shown in Fig. 1, all the characters of Stokes curves are *uniquely determined* only by requiring the univaludness condition. Remerkably, to preserve univaluedness on the whole plane, it can happen that even ordinary Stokes curves become broken ones, meaning that the connection does not occur on this segment even though they are ordinary Stokes curves. So, we learn from this example that broken segments are not limited to the new Stokes curve, and that the resulting Stokes geometry totally bears *global* topology of the Stokes graph. It is not enough to focus on a certain limited part.

Next we present the Stokes geometry for the $n = 4$ case. The algorithm to draw ordinary and new Stokes curves together with ordinary and virtual turning points are the same as $n = 3$ case. The number of saddle point solutions is 8. The numbers of ordinary and new Stokes curves are 42 and 21, respectively. In Fig. 4, we show the Stokes graphs for $c = 1$, $q_0 = 0$. It is hard to distinguish in the figure, but we should note that two ordinary and two new Stokes curves are quadruply degenerated on the $\mathrm{Re}\, q_4$ axis. As the case of degenerated Stokes lines observed in the graph for $n = 3$, these degenerated Stokes lines do not cause any complexity in the final Stokes geometry because all the Stokes lines are those between different saddles, i.e., they are all independent each other.

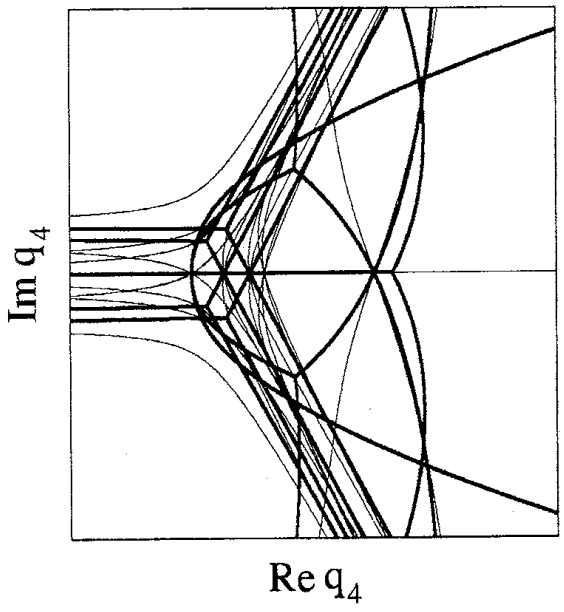

Figure 4: A Stokes graph for 3-step Hénon map propagator with $c = 1, q_0 = 0$. Ordinary and new Stokes curves are drawn as thick and thin lines, respectively. Ordinary and virtual turning points together with Information on the connection are not shown here.

As in the case of $n = 3$, considering simple crossing points is not enough to complete the Stokes geometry. On the $\mathrm{Re}\, q_4$ axis, there are several degenerate crossing points.

In Fig. 5, we present Stokes geometry around such degenerated crossing points on the $\mathrm{Re}\, q_4$ axis. These four crossing points are those appearing in the magnified graph given as Fig. 4. Similarly to single crossings, it is easy to verify that all the characters of the Stokes curves around degenerated crossings are uniquely determined as long as characters of the half of the segments, i.e., six segiments, are already known. For example, in case Fig 5(a), three ordinary curves, $(1 \cdot 7)$, $(4 \cdot 6)$, $(6 \cdot 7)$, and three new Stokes curves, $(1 \cdot 4)$, $(4 \cdot 7)$, $(1 \cdot 6)$, are involved in the connection. For each Stokes curve, character of each segment in either side is already known because of the rule around ordinary or virtual turning points. Using these data, it is easy to check that the extension beyond the crossing point is unique. The same is true in other crossings shown in Fig. 5. All the degenerated crossing points appearing in Fig. 4 can be treated in the same manner.

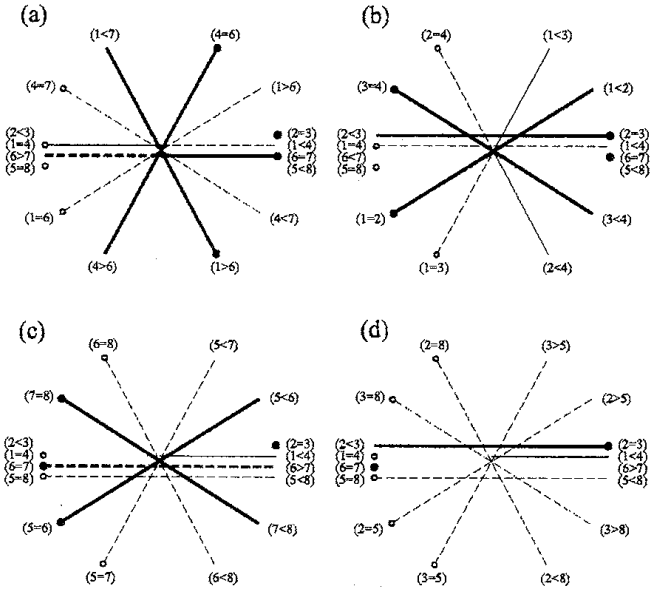

Figure 5: Connection around degenerated crossing points in the case with $n = 4, c = 1, q_0 = 0$. (a), (b), (c) and (d) respectively correspond to the crossing points a, b, c and d shown in Fig. 6. Thick and thin lines stand for the ordinary and new Stokes curves. Gray ones represent Stokes lines that are not involved in the connection around the crossing point under consideration.

4. Validity of Stokes geometry

As mentioned, univaluedness is a necessary condition for the connection problem to be consistent. If this consistency is violated, there should exist some unknown ingredients other than virtual turning points and new Stokes curves, etc., but at least all the Stokes graphs examined so far do not only violate this condition but also the resulting geometries are unique.

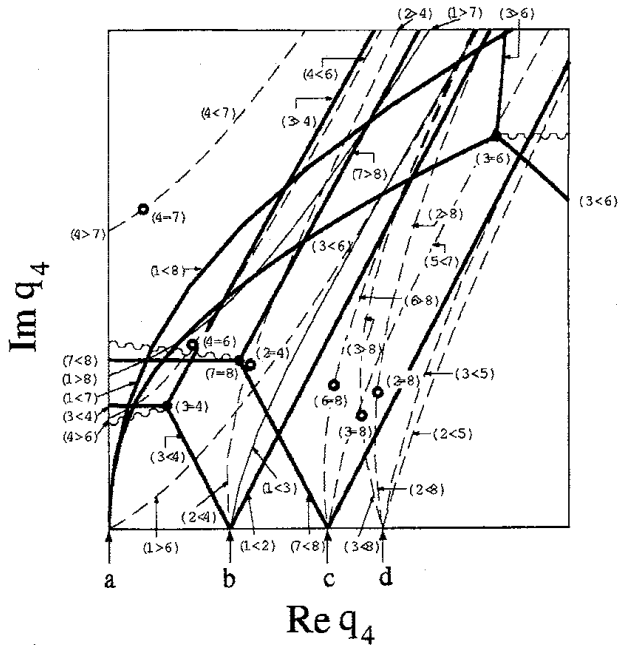

Figure 6: Magnification of a part of Stokes geometry for $c = 1, q_0 = 0$. The solid and open circles denote the ordinary and virtual turning points respectively. Ordinary Stokes curves are drawn as thick lines and new ones as thin lines. The broken segments represent the parts of Stokes curves on which where no connections occur.

In this section, we shall see the validity of a concrete example of Stokes geometry obtained in the previous section by using hyperasymptotic expansions for multiple integrals [18, 12]. Hyperasymptotic expansions are a systematic re-expansion of the remainder terms around the solutions not involved in the original expansions, and they essentially improve the Poincarè-type asymptotics. This would be closely related to the exact WKB analysis previously discussed, and also recent development of the exact steepest descent method [17].

Hyperasymptotic expansions generate exponentially improved numerical accuracy; this is because expansions incorporate non-local natures of asymptotic expansions, and exactly this fact will be used to analyse the Stokes geometry. The idea behind this is that the reason for divergence of asymptotic expansions of integrals around a certain sadde is due to the existence of other saddles, and just for this reason the saddles should be related to each other in a consistent manner.

Here we only give a brief sketch of how hyperasypmotic expansions can be utilized to check the validity of Stokes geometry [12]. Consider the Laplace-type integral

$$I^{(n)}(\eta) = \int_{\mathcal{C}_n} dz g(z) \exp\Big\{-\eta f(z)\Big\}, \tag{16}$$

where we assume that the function $f(z)$ has simple saddle points denoted by $\{z_n\}$, and that the contour line here represented by $\mathcal{C}_n$ expresses a steepest descent path which

connects vallays $\mathrm{Re}\{\eta[f(z)-f_n]\}$ and passes through a saddle z_n. Then we write the asymptotic expansion of the integral $I^{(n)}(\eta)$ with repsect to a large parameter η as

$$I^{(n)}(\eta)=\frac{\exp\{-\eta f(z_n)\}}{\sqrt{\eta}}\sum_{r=0}^{N-1}\frac{T_r^{(n)}}{\eta^r}+R^{(n)}(\eta,N). \tag{17}$$

Here $T_r^{(n)}$s denote coefficients of the asymptotic expansion around the saddle z_n, and $R^{(n)}(\eta,N)$ the remainder of the expansion up to the degree N.

A crucial step to see this is to re-express the remainder term $R^{(n)}(\eta,N)$ in terms of $T_r^{(m)}$ that are the asymptotic coefficients of saddles m not involved in the initial expansion. This leads to a sequence of the so-called *hyperseries*

$$\begin{aligned}T^{(n)}(\eta)=&\sum_{r=0}^{N_n-1}T_r^{(n)}K_r^{(n)}+\sum_{m_1}C_{nm_1}\sum_{r=1}^{N_{nm_1}-1}T_r^{(m_1)}K_r^{(nm_1)}\\&+\sum_{m_1}\sum_{m_2}C_{nm_1}C_{m_1m_2}+\sum_{r=0}^{N_{m_1m_2}-1}T_r^{(m_2)}K_r^{(m_1m_2)}+\cdots\\&+\sum_{m_1}\cdots\sum_{m_M}C_{nm_1}C_{m_1m_2}\cdots C_{m_{M-1}m_M}\Big(\sum_{r=0}^{N_{n\cdots m_M}-1}T_r^{(m_M)}K_r^{(nm_1\cdots m_M)}+R^{(nm_1\cdots m_M)}\Big).\end{aligned} \tag{18}$$

Here $K_r^{(nm_1\cdots m_p)}$s are called *hyperterminants* which are universal multiple integrals not depending on the original integral [18]. The coefficients C_{nm} inserted in front of each contribution carry information regarding the Riemann sheet structure of the Borel plane on which the singularities corresponding to the saddles n and m are located. Hence, the coefficients C_{nm} have key information as to Stokes phenomena, and one can assign the following possible values,

$$|C_{nm}|=\begin{cases}1 & z_n \text{ is adjacent to } z_m\\ 0 & z_n \text{ is not adjacent to } z_m\end{cases}$$

where *adjacency* is introduced to represent that there exists a common steepest descent contour between the saddles z_n and z_m as one rotates the argument of η from 0 to 2π [18]. Information on Stokes geometry in this context is thus reduced to determining the coeffienet C_{nm}. The idea developed by Olde Daalhuis for differential equations, and later applied by Howls for multiple integrals concernes how one derives a set of algebraic equations to determine C_{nm} [19, 12].

The idea using hyperasymptotic expansions to determine the Riemann sheet structure is available in our quantum propagator for the Hénon map. What we have to prepare is asymptotic coefficients for each classical solutions and a set of hyperteminants. We have used an efficient algorithm to compute hypertaminants developed in [20]. As for the asymptotic coefficients $T_r^{(n)}$, we here explicitly express them in case of 2-step quantum propagator;

$$I(q_0,q_3)=\int_{-\infty}^{\infty}\int_{-\infty}^{\infty}dq_1dq_2\exp\Big[\eta S(q_0,q_1,q_2,q_3)\Big], \tag{19}$$

where the action functional is given as,

$$S(q_0,q_1,q_2,q_3)=\frac{1}{2}(q_3-q_2)^2+\frac{1}{2}(q_2-q_1)^2+\frac{1}{2}(q_1-q_0)^2+cq_2+\frac{q_2^3}{3}+cq_1+\frac{q_1^3}{3}. \quad (20)$$

This admits asymptotic expansion as

$$I(q_0,q_3)=\frac{\exp\{-2\eta(\alpha+\beta)/3\}}{\eta}T^{(n)}(\eta) \quad (21)$$

with coefficients,

$$T_r^{(k)}=\sum_{l_1+l_2+l_3+l_4=2r} i^{r+1}\frac{\prod_{i=1}^4 R_i^{l_i}}{\prod_{i=1}^4\Gamma(l_i+1)}\frac{\Gamma((p+1)/2))\Gamma((q+1)/2)}{\lambda_1^{(p+1)/2}\lambda_1^{(q+1)/2}}, \quad (22)$$

where

$$p=3l_1+l_2+2l_3,$$
$$q=2l_2+l_3+3l_4.$$

λ_is' are eigenvalues of the matrix;

$$A^{(k)}=\begin{pmatrix} 1+q_1^{(k)} & -\frac{1}{2} \\ -\frac{1}{2} & 1+q_2^{(k)} \end{pmatrix}$$

and $R_i s'$are quantities expressed using the eigenvector of A.

An example we now examine has a set of the same parameter values taken in Fig. 1. In particular, we analyze the connection around a degenerated crossing point on the $\mathrm{Re}\, q_3$ axis. As argued previously, it plays a key role in completing the Stokes geometry, since the connection around the rest of crossing points cannot be fixed until this degenerated crossing point is solved.

We have evaluated the coefficients C_{nm} just on the Stokes curves between the saddles n and m, and checked whether these saddles are on the same Riemann sheet or not. The number of terms in each branch of the tree-tpye expansion (18) is given by the following recursive rule [19, 12]:

$$\begin{aligned} N_n &= \min_{m\neq n}\{2\eta|S^{(n)}-S^{(m)}|\} \\ N_{nm_1} &= \max\{0, N_n-\eta|S^{(n)}-S^{(m_1)}| \\ N_{nm_1m_2} &= \max\{0, N_{nm_1}-\eta|S^{(m_1)}-S^{(m_2)}| \\ &\cdots \end{aligned} \quad (23)$$

From this rule, we notice that if $|S^{(n)}-S^{(m)}|$ for a certain pair of saddles n, m is sufficiently small as compared to those for all other pairs, only this (n,m) pair actually appears in the expansion (18), and the other branches contain null terms. In this case, we easily evaluate the coefficient C_{nm} by solving the algebraic equation in which only C_{nm} is an unknown variable. In order to see the adjacency relation between the saddle n and m, we can use this fact: $|S^{(n)}-S^{(m)}|$ can be adjusted as small as we wish by

taking q_3 close to the turning point since $|S^{(n)} - S^{(m)}| = 0$ just on the turning point between the saddle n and m.

Indeed, as shown in Fig. 7, we could compute the coefficients C_{nm} around the degenerated crossing for the points close to the turning points. C_{12} and C_{23} concern the Stokes curves emanating from ordinary turning points. According to the accuracy estimation [21, 19], we can set $C_{12} = C_{23} = 1$ unambiguougly. This result is consistent with the fact that the corresponding Stokes curves emanating from ordinary turning points are *solid*. Also, from the numerical calculated values for C_{14} and C_{13}, we can assign C_{14} and $C_{13} = 0$. These are consitent with the broken Stokes curves emanating from virual turning points.

Even beyond the degenerated crossing point, if we limit ourselves to the Re q_3 axis, it is possible to evaluate the coefiicients. The results for C_{14} and C_{23} are again consistent with predicted characters of ordinary and new Stokes curves. The Stokes curve between 2 and 3 does not change its character, but the new Stokes curve emanating from the turning point $(1 = 4)$ changes from broken to solid as predicted.

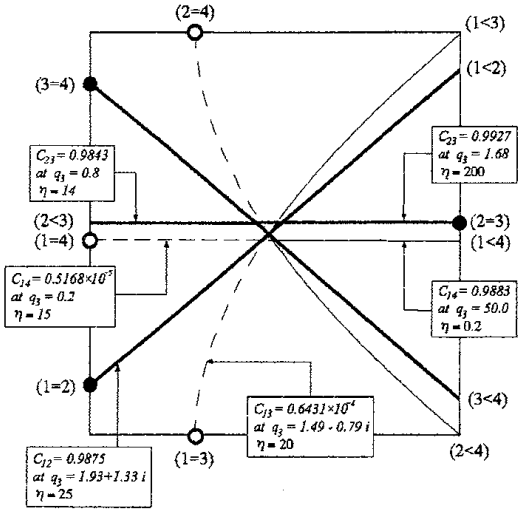

Figure 7: The coefficients determining the Riemann sheet structure around the degenerated turning point. The range of magnification and the parameter values are the same as Fig. 3. In each box, we denote the coefficient between the saddle i and j by C_{ij} and it is evaluated at a subsequent point q_3 with η specified in each box. Note that the positions shown by arrows are not necessarilly correct points at which the coefficients are evaluated.

Unfortunately, it is a highly laborious task to determine adjacency on the rest of Stokes curves beyond the degenerated crossing point because we need to enter into a very deep hierarchical level in the hyperseries (18). For example, let us consider a certain point on the new Stokes curve $(1 < 3)$, which is located on the opposite side to the turning point $(1 = 3)$ with respect to the degenerated crossing point. As shown in the diagram (8), in order to make C_{13} appear in the truncated hyperseries, we have to start the expansion either from the saddle $n = 1$ or $n = 4$ otherwise the truncation

terminates without picking up C_{13}. However, if we choose $n = 4$ as a base saddle, $N_4 = 40$ results from the rule (23), then the expansion is truncated before appearing C_{13}. On the other hand, if $n = 1$ is chosen as a base saddle, $N_1 = 110$ and the desired C_{13} certainly appears as the first level of hierarchy. However, the expansion in this case continues up to very deep levels since the paths reflecting between 2 and 3 many times do not gain so many terms and therefore require very higher order hyperseries, that necessarily involves very higher order hyperterminants. The situation at the other points on the same Stokes curves and also those on the ordinary Stokes curve ($1 < 2$) is similar.

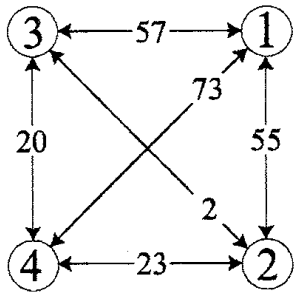

Figure 8: Action difference $|S^{(i)} - S^{(j)}|$ between the saddle i and j. The values shown in the diagram are the ones multiplied by $\eta = 20$. The number inside the circle represents the number of saddle.

5. Concluding remarks

In the present note, we have studied Stokes geometry of quantized Hénon map by following recently proposed prescriptions based on the exact WKB analysis. As mentioned, a primary motivation of our work originates from a recent success of complex semiclassical description of quantum tunneling especially in the presence of chaos [6, 10]. In such a program, the understanding of Stokes phenomena is a crucial step to make our analysis self-containd. The strategy we took first was to select out the simplest possible chaotic system suitable for our purpose. The Hénon map would be the best possible candidate that meets such a requirement.

The first task we presented here was to establish the definition of turning points and Stokes curves, which are the most relevant ingredients to construct the Stokes geometry. Fortunately, recent progresses of the exact WKB analysis are quite helpful and has provided concrete procedures to do so and established several relevant facts. We could define Stokes graphs on the same line as the case of higher order differential equations by deriving the differential operators acting on our multiple integrals. We can show, though not explicitly presented here, that deriving differential equaitons is equivalent to solving an initial value problem of the Hénon map [15]. Virtual turning points as well as new Stokes curves were then introduced.

With these settings, Stokes graphs for 2 and 3 step Hénon map propagators were drawn, and the corresponding Stokes geometry was discussed under the priciple of the

univaluedness condition on given Stokes graphs. Several concrete examples studied in the present paper provide unique geometry althouth, in principle, arbitrary combinations of turning points and Stokes lines do not necessarily fix Stokes geometry uniquely.

In order to verify that resulting Stokes geometry is correct, hyperasymptotic expansions were considered. A set of algebraic equations with controllable errors was used to explore the Riemann sheet structure of the Borel transform or equivalently adjacency relation of saddles of our multiple integrals. The results were entirely consistent with those determined through the univaluedness condition.

We should mention that the present analysis is still a first step towards our final goal, and a lot of significant but unsolved problems remain. The most urgent issue would be to make clear the relation between classical dynamics generating chaos and the corresponding Stokes geometry. In the classical side, stretching and folding is a key mechanism generating chaos, and the number of folding points of the Lagrangian manifold increases exponentially as a function of time. The folding points of the Lagrangian manifold manifest themselves as the turning points in Stokes geometry. Three Stokes curves emanate from a simple turning point, and local Stokes geometry in the vicinity of folding points can be well understood within conventional arguments. However, because of the crossing of Stokes curves and resulting complicated Stokes graphs, we cannot avoid taking into account global aspects of geometry, and it is difficult to give an intuitive mapping relation connecting the structure of Lagrangian manifolds and the corresponding Stokes geometry.

In order to go beyond it, analyzing Stokes geomety in the anti-integrable limit would be the first target to be investigated. If the situation for the anti-integrable limit is understood, one way to step forward is to trace Stokes geometry as a function of the system parameter, and focus on bifurcation phenomena [22, 15]. In the horseshoe case, all the turning points are located on the real plane, but as the nonlinear paremeter c decreases, some of them fall into purely imaginary plane. Such an event occurs as a result of coalescence of turning points. If we know how the Stokes graph changes when such a bifurcation phenomenon occurs, the Stokes geometry in a generic parameter value can be traced from the anti-integrable limit in principle. This is exactly the same strategy to study the *pruning* of the horseshoe structure [23].

0.1 Acknowledgments

The author is grateful to T. Aoki, A. Olde Daalhais, C.J. Howls, T. Kawai, T. Onishi, Y. Takei, and A. Voros for their valuable comments and discussions. This work is based on the collaboration with K.S. Ikeda, which is announced as ref. [15].

References

[1] S. Friedland and J. Milnor, Ergod. Theor. Dyn. Sys. **9**(1989)67.

[2] M. Tabor, Physica D **6** (1983) 195.

[3] M.J. Davis and E.J. Heller, Chem. Phys. **75** (1981), 246.

[4] S. C. Creagh, in *Tunneling in complex systems* ed. by S. Tomsovic (World Scientific, Singapore, 1998) 35.

[5] O. Bohigas, S. Tomsovic and D. Ullmo Phys. Rep. **223**(1993)43; S. Tomsovic and D. Ullmo Phys. Rev E **50**(1994)145.

[6] A. Shudo and K. S. Ikeda, Phys. Rev. Lett. **74**, 682 (1995); Physica D**115**, 234 (1998); T. Onishi, A. Shudo, K.S. Ikeda, and K. Takahashi, Phys. Rev. E **64**, 025201(R) (2001).

[7] K. Takahashi and K. S. Ikeda, Ann. Phys. (NY) J. Phys. A. **283** 94; J. Phys. A **36** (2003) 7953.

[8] E. Bedford and J. Smillie, Invent. Math. **103**(1991)69; J. Amer. Math. Soc. **4**(1991)657; Math. Ann. **294**(1992)395; E. Bedford M. Lyubich and J. Smillie, Invent. Math. **112**(1993)77;

[9] J.E. Fornæss and N. Sibony, Duke Math. J. **65** (1992) 345.

[10] A. Shudo, Y. Ishii and K.S. Ikeda, J. Phys. A. **35** (2003) L225; A. Shudo, Y. Ishii and K.S. Ikeda, to be submitted.

[11] C. M. Bender and T. T. Wu, Phys. Rev., **184**, 1231 (1969); A. Voros, Ann. Inst. Henri Poincaré, **39**, 211 (1983); J. Zinn-Justin, J. Math. Phys., **25**, 549 (1984); H. J. Silverstone, Phys. Rev. Lett., **55**, 2523 (1985); E. Delabaere, H. Dillinger et F. Pham, Ann. Inst. Fourier, **43**, 433 (1993); T. Kawai and Y. Takei, Algebraic Analysis of Singular Perturbations. (Iwanami, 1998. In Japanese and its translation will be published by AMS in 2004).

[12] C.J. Howls, Proc. R. Soc. Lond. A, **453**(1997)2271.

[13] T. Aoki, T. Kawai and Y. Takei, in Analyse algébrique des perturbations singulières. I. (ed. by L. Boutet de Monvel) Hermann, (1994) 69.

[14] H.L. Berk, W.M. Nevins and K.V. Roberts, J. Math. Phys., **23**(1982) 988.

[15] A. Shudo and K.S. Ikeda, to be submitted.

[16] This equation has first been derived by T. Aoki in a heuristic way.

[17] T. Aoki, T. Kawai and Y. Takei, J. Math. Phys. **42** (2001) 3691.

[18] M.V. Berry and C.J. Howls, Proc. L. Soc. London, **430** (1991) 653; M.V. Berry and C.J. Howls, Proc. L. Soc. London, **434** (1991) 657.

[19] A. B. Olde Daalhuis, Proc. R. Soc. London **454** (1998) 1.

[20] A.B. Olde Daalhuis, Method Appl. Analysis, **2**(1995)198; J. Comp. Appl. Math. **76**(1995) 255.

[21] A.B. Olde Daalhuis and F. W. Olver, Methods Appl. Analysis **2** (1995) 173.

[22] T. Aoki, T. Kawai, S. Sasaki, A. Shudo and Y. Takei, *Virtual turning points and bifurcation of Stokes curves for higher order ordinary differential equations*, preprint.

[23] Cvitanović P, Gunaratne G and Procaccia I, Phys. Rev. A **38** (1988) 1503.